Standup time Estimation of Undercut Moist Sand Slope Using Numerical Simulations

Laddawon Dul* and Cheowchan Leelasukseree

Department of Mining and Petroleum Engineering, Chiang Mai University, Chiang Mai, THAILAND
**Corresponding author; E-mail address: Laddawon_dul@cmu.ac.th*

Abstract

Undercut slope is defined as a slope, which is excavated at its toe. An undercut slope would be failed if undercut width is equal to or greater than its maximum undercut width. Sometimes, the undercut slope is temporarily stable. The undercut slope could displace slowly over a period and it finally fails. The period of undercut slope in stable is called standup time. In this paper, the standup time was estimated by using numerical simulations. A series of numerical simulations using 3DEC was performed to study of standup time of undercut slopes. The numerical models were applied the physical properties and creep parameters of moist sand, which were tested in laboratory. Mohr-Coulomb and Burgers model were assigned to the numerical simulations. The slope inclination of the numerical models was varied. The slope inclinations were 50^{o}, 30^{o}, 18^{o} and 15^{o}. The undercut slope models showed a relationship between slope inclination, undercut width and standup time. When the slope inclination was shallower than the friction angle of bedding plane, its standup time and undercut width were longer and wider than the steeper. The slope inclination was inversely proportional to undercut width while the undercut width was proportion to the standup time.

Keywords**:** standup time, Burgers creep model, undercut slope.

1. Introduction

Undercutting is a cause of slope failures when slopes are undercut at the toe. When undercut, the stresses on the slope are re-aligned from the center to the sides, called arch action. The major principal stress in tangential direction supports the arch and the minor principal stress in radial direction confines the arch stack [1]. The stresses in arch action of the undercut slope were studied by using a series of physical models [2]. The physical models were consisted of moist sand mass on a low friction angle bed. The creep deformations in the physical models have been excluded in the previous studies.

In this paper, creep deformation of undercut slopes was primarily studied by using a set of numerical models. 3DEC was employed to model the physical models of the earlier studies. 3DEC is a three-dimensional distinct element program, which is a tool for this study and able to give solution for static analysis in geomechanics.[3]. The assigned physical properties including creep properties for the numerical models were determined in laboratory tests. Results of the numerical analysis were expected that the changes of stresses and creep deformations of stable undercut slopes would be unveiled. These numerical model results could make a better understand the effect of slope inclination and undercut width to the standup time of the undercut slope.

2. Background.

2.1 Elastic and plastic deformation

Materials in the elastic region have no deformation when their applied stress are total removed. The materials are still intact [4]. This elastic behavior is able to present in stress-strain curve, which is only a linear portion at low stress. When the stress is more applied to material, the material behavior becomes to plastic. The material deformation is irrecoverable.

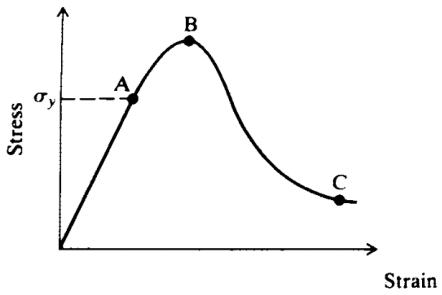

Fig.1 Relationship of stress-strain curve [5]

The Fig 1 shows the stresses-strain relationship of a material. The linear elastic deformation starts when the material is loaded until point A. Beyond point A, the material deformation is the plastic deformation before point B. Point B is the peak strength of the material, which the failure occurs [5].

2.2 Creep deformation

The creep behavior is material deformation over time when the material is loaded. For example, a material is loaded with a constant applied stress. The material deformation magnitude slowly increases for a time extent. Finally, the material is damaged and failed. A general strain-time curve, sometimes called creep cure, under constant of applied stress is shown in Fig 2. This curve has three-state of creep behavior, which are primary, secondary and tertiary states, respectively.

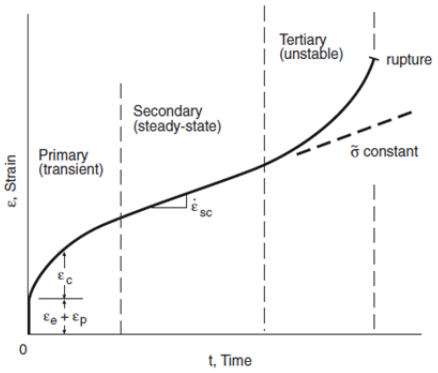

Fig.2 Model of the creep deformation and time [4]

The creep curve starts at nearly an instantaneous elastic strain. The stress is applied and held constants that strain is in transient or primary state. The strain in this state is a summation of elastic and plastic strains. The creep rate is gradually decreased and converges to the minimum rate in this state.

In the secondary or steady state, the curve has a constant rate, which corresponds to a constant curve slope. The strain rate is very low. At tertiary stage transition, the strain rate increases rapidly, or the material is quickly deformed and finally ruptures [6].

2.3 Linear visco-elastic model.

The linear visco-elastic is composed of springs and despots. Burgers model is a popular of the linear visco-elastic models. Four Bergers' creep constants were practically determined in laboratory.

According to linear elasticity, there are two elastic constants that are bulk (K) and shear (G) moduli. Burgers model is Maxwell and Kelvin bodies in series and, as a result, consists of two shear moduli and two dashpots. The Fig 3 exhibits the creep model of Burgers and its four-constants.

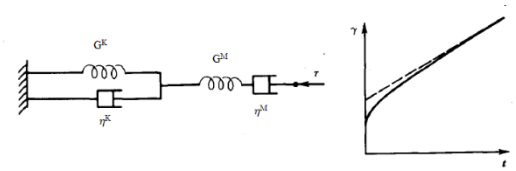

Fig.3 Burger's model [7].

The Burger's body is subjected a constant axial stress ($\boldsymbol{\sigma}$) and this is related the axial strain with time ($\boldsymbol{\varepsilon}^{B}_{(t)}$). The equation of Burgers model represents from elastic and visco-elastic behavior as shown below [7]:

$$\varepsilon^{B}_{(t)} = \frac{\sigma}{3G^{M}} + \frac{\sigma t}{3\eta^{M}} + \frac{\sigma}{3G^{K}}\left(1 - e^{-\left(\frac{G^{K}t}{\eta^{K}}\right)}\right) + \frac{2\sigma}{9K} \quad (1)$$

Equation 1 defines four creep parameters for fitting creep curve which are shear modulus of Maxwell body (G^{M}), shear modulus of Kelvin body (G^{K}), dynamic viscosity (η^{M}) and visco-elastic coefficient of Kelvin body (η^{K}).

2.4 Numerical simulations

Mechanical behavior of materials is possibly obtained by using numerical simulations. A series of numerical simulation was utilized to study the creep behavior of the undercut slope. The stresses and displacements of the numerical models can be exhibited at any point. The models can be divided into zones and assigned different material models and properties [8].

3DEC program is a three-dimension with district element method and used in this study. 3DEC is based on dynamic (time-domain with the mechanical interaction between blocks). The solution is finite difference method to motion law equation for the block system. The motion law and the constitutive equation are applied into system at each time step. The Fig 4 illustrates the mechanical calculation cycle in a time step [3].

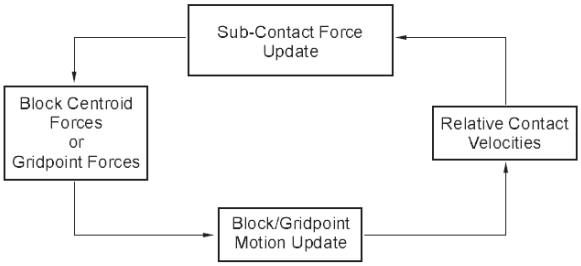

Fig.4 Mechanical calculation cycle [3].

3. Methodology.

The numerical simulations' dimensions using 3DEC in this study were based on the physical models [2]. The study was combined with three parts, which were laboratory tests, determination of creep parameters and numerical simulations.

3.1 Laboratory tests

3.1.1 Uniaxial Compressive Strength (UCS) tests.

Material's elastic modulus was determined from the unconfined compressive strength test. The test was unconsolidated-undrained test that drainage at any stage was disallowed [9]. The test sample was silica sand no.6 with controlling moisture content at 10% and 1,395 kg/m^3 of density. The moist sand was remolded in cylindrical shape, 5 cm in diameter and 10 cm height.

The average UCS strengths of moist sand samples was 2.02 kPa. The average Young's moduli of moist sand samples were 106.9 kPa. Later, Young's modulus from the laboratory test was input in the numerical simulations.

3.1.2 Direct shear test

The sample size for direct shear test was 6 cm in diameter and 2 cm in thickness. Same as UCS test, silica sand no.6 with 10% moisture content was remolded and prepared to have sample density at 1,395 kg/m3. The direct shear test results were used to determine cohesion and friction angle of the moist sand samples. Cohesion and friction angle were derived from a linear relationship between normal stress and shear stress during shearing.

The basic engineering properties was attained from the results of the laboratory tests. Young's modulus from the UCS tests was input in Equation 2 to obtain bulk (K) and shear (G) moduli. It is noted that Poisson's ratio (υ) was assumed as 0.3. Table 1 summarizes all basic physical properties of moist silica sand from laboratory tests.

$$K = \frac{E}{3(1-2\upsilon)} \quad \text{and} \quad G = \frac{E}{2(1+\upsilon)} \tag{2}$$

Table 1 Basic physical properties of moist silica sand from laboratory tests.

Bulk density (ρ) kg/m^3	1,395
Water content (w) %	10%
UCS (kPa)	2.02
Young's modulus, E (kPa)	106.9
Bulk elastic modulus, K (kPa)	89.08
Shear elastic modulus, G (kPa)	41.12
Internal friction angle (ϕ)	38.62
Apparent cohesion, Si (kPa)	2.24
Tension (kPa)	1.40

3.1.3 Uniaxial compression creep tests.

Moist sand core samples, same UCS sample size, were used in uniaxial creep tests. This test was performed for studying creep behavior and determining strain rate as function of time. Based on UCS of the moist sand, the short term creep test needs an applied axial load that ranges 50% - 80% of its UCS. The long term creep test must apply approximately 15% - 40% of UCS. In this paper, the long term creep test has been focused.

3.2 Determination of creep parameters.

Based on the uniaxial compression creep test results, the axial strain and time were plotted as strain-time curves. The strain - time curves from creep tests were used to calculate four important creep constant parameters of Burgers visco-elastic model. These four constants were required for numerical simulations to estimate standup time of undercut moist sand slope. The uniaxial compression long term creep tests had been conducted. The tested data points were fit in strain and time space as show in Fig. 5.

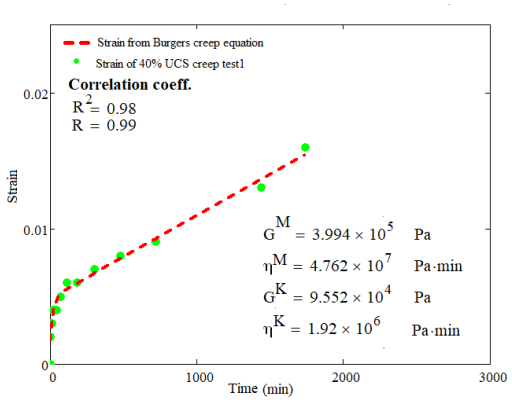

Fig. 5 Creep test data points and best fit of Burger's creep model.

The four constants of Burgers creep model from the tests were the important input parameters for the numerical simulations. The summary of the required input parameters is shown in the Table 2.

3.3 Numerical modeling.

The estimation of standup time used 3DEC by simulating creep behavior of moist sand slope when undercut. The numerical model was constructed after Pipatpongsa's physical models [1]. The physical model was made of moist sand and placed on an inclined rigid bed with side supports. The model's shape and dimensions are displayed in Fig. 6. It is noted that a low interface friction angle between the moist sand and the inclined bed was 18.5°, based on a study of silica sand no.6 by Ouch, et al., 2015 [10].

Table 2 Burgers creep input parameters for 3DEC.

Parameters of Burgers creep	Model
Density (kg/m^3)	1,395
Bulk elastic modulus, K (kPa)	89.08
Shear modulus in Maxwell body, G^M (MPa)	0.40
Dashpots dynamic viscosity, η^M (MPa*min)	48.77
Shear modulus in Kelvin body, G^K (MPa)	0.06
visco-elastic coefficient in Kelvin body, η^K (MPa*min)	2.75

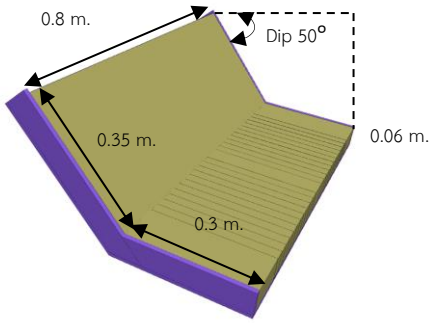

Fig. 6 Model of slope inclination angle at 50°

The models were constructed in four different dip angles of inclined rigid bed or slope. The inclinations of slope were 50°, 30°, 18° and 15°. The Fig 7 shows the procedure of numerical analyses in this study.

The Mohr-Coulomb model was assigned to determine the maximum undercut width. During undercut, the principal stresses in the slope were realigned. The principal stresses formed an arch action during undercutting.

For time dependent analyses, the slopes had different standup time, depended on the slope inclination, stresses in the slope, and assigned material properties. Burgers visco-plastic and Mohr-Coulomb models were applied to estimate standup time for long term creep models.

After the model construction completed, a series of numerical simulations were executed to determine the maximum undercut width by using Mohr-Coulomb model and estimate their standup time. Stresses and displacements of 10 observation points, as shown in Fig 8, in the model were acquired and recorded.

Stresses at the observation points, computed by 3DEC, were post-processed and transformed in dip vector and strike directions of the undercut slope. The transformed stresses and displacements were used for further investigation of the undercut slope numerical analyses and their standup time.

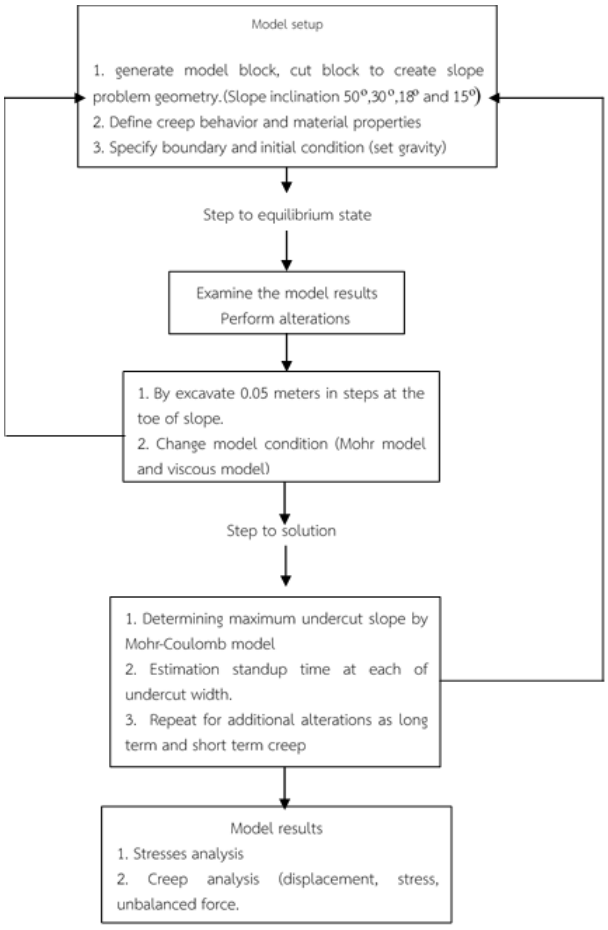

Fig. 7 Procedure of numerical analyses.

4. Numerical simulation results

The numerical simulations used Mohr-Coulomb and Burgers visco-plastic models. The Mohr-Coulomb model was assigned to determine the maximum undercut width of each inclination angle. Next, Mohr-Coulomb and Burgers visco-plastic models were used to numerically estimate the stand-up time of each moist sand slope at its various undercut width.

4.1 The influence of undercut width and slope inclination.

After the models were completely constructed, each model was sequentially undercut to determine its maximum undercut width. As stated before, there were 4 models that had different slope inclination angles e.g. 50°, 30°, 18° and 15°. During the analyses, stresses and displacements at the observation points were digitally recorded. These observation points were located as in Fig 9.

After the completion of the sequential undercut, the maximum undercut widths of the models at slope inclination 50°, 30°, 18° and 15° were 0.35, 0.55, 0.8 and 0.8 m, respectively. It is clearly that the maximum undercut width was affected by the slope inclination and interface friction angle between the moist sand and the inclined bed. The wider undercut width had more extent when the slope inclination was shallowed. When the inclination angle was less than the interface friction angle between the moist sand and the inclined bed, the slope toe was totally undercut, and the slope was still in stable.

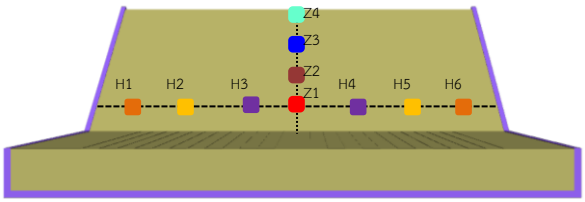

Fig.8 Location of 10 observation points.

To investigate the relationships between slope inclinations, undercut width and stresses, the stresses on the observation points along centerline of the models were post-processed. Fig. 9 presents tangential radial and tangential stresses of 50° slope inclination model at the observation points from initial to the maximum undercut widths.

The plots illustrate magnitude of radial and tangential stresses at the slope centerline and the unbalanced force. The unbalanced force converged to zero that was able to imply the model in stable. When the slope was additionally undercut, the unbalanced force was suddenly increased then sharply dropped and approached to zero again. The radial stresses were decreased inversely with the undercut span width. While the stresses were accumulated in tangential direction. At some undercut width, the tangential stress was however dropped due to the arch crown upward shifting.

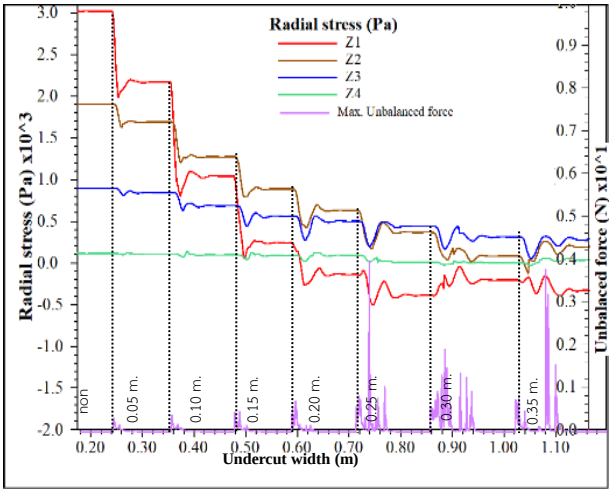

a) Radial stress.

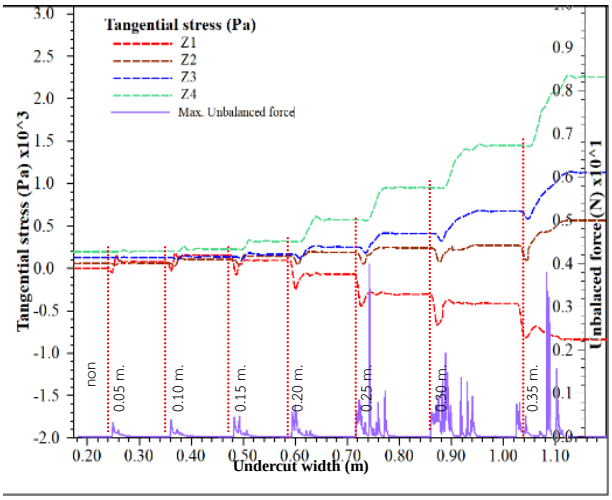

b) Tangential stress.

Fig. 9 Radial and tangential stresses of each undercut span of 50° slope inclination.

Fig. 10 shows a stereographic projection of the direction of the principal stresses in an area near Z3 point. The plot unveiled that the directions of the major and minor principal stresses were in dip vector and strike of the slope, respectively. The intermediate principal stress direction was upwardly normal to the bed.

When the slope was undercut, the major and minor principal stresses were altered in magnitude and directions. The

directions of the major and minor principal stresses were switched and became the tangential and radial stresses, respectively. At the maximum undercut span, the directions of the major and minor principal stresses were plotted in Fig. 11.

According to the previous studies [1, 2], the major principal stress supported the slope and its direction was changed in the circumferential of the arch. While the minor principal stresses confined the arch and aligned in radial direction. The arch formation was induced by uneven displacements across the undercut slope. Fig 12 shows the uneven displacement of the undercut slope at inclination 50^{o} and 0.35 m undercut width.

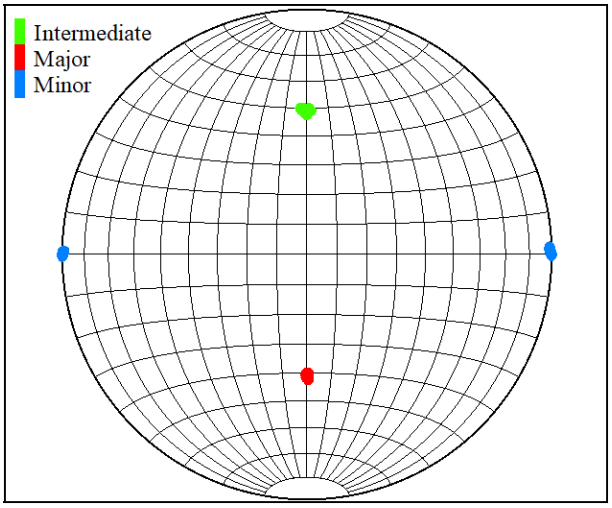

Fig. 10 Stereographic projection of principal stress directions of non-undercut at 50^{o} slope inclination at point Z3 (lower hemisphere)

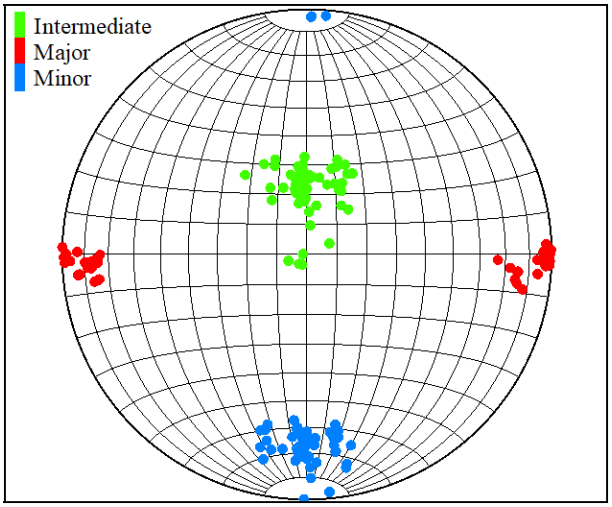

Fig. 11 Stereographic projection of principal stress directions of 0.35 m undercut width at 50^{o} slope inclination at point Z3 (lower hemisphere).

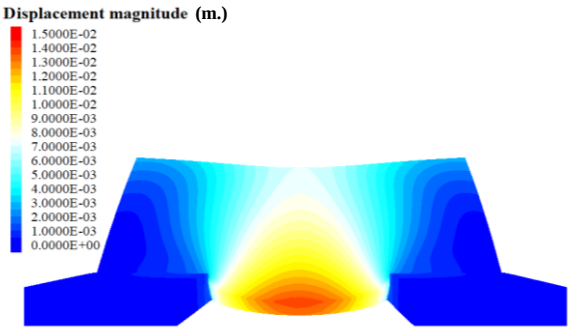

Fig. 12 Displacement magnitude of 0.35 m undercut width at 50^{o} slope inclination (with Mohr- Coulomb model).

4.2 Standup time estimation

The numerical simulations with Burgers creep model were analyzed to find the standup time after undercut at the various undercut widths. The creep curve presented the displacement of points Z1 to Z4 on middle of slope. The standup time was estimated from the creep curve by find the beginning of the tertiary stage. Fig. 1 3 presents a creep curve of undercut width 0.3 m of Series 1 and its unbalanced force.

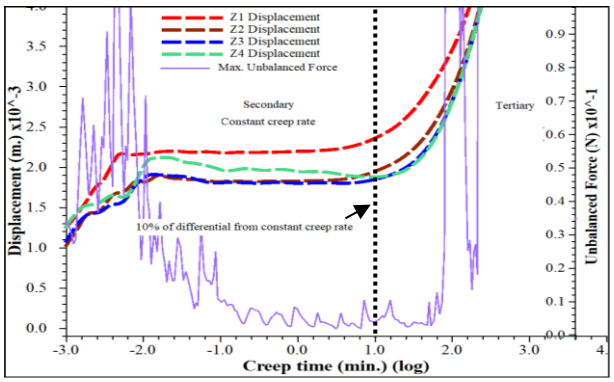

Fig. 13 Creep curve of Series 1 - slope incline 50^{o} at undercut width 0.3 m.

From Fig. 13, the model's unbalanced force kept decreasing and stayed at a low magnitude in the secondary stage. The displacement became constant. At the end of the secondary stage, both the unbalanced force and the displacement of the model drastically increased. These unbalanced force and displacement escalations would be a sign that the model shifted from the secondary to tertiary stages. In this study, a point on creep curve that the model transformed secondary to tertiary stages had, assumedly, creep rate 10% increase. For example, the vertical black dashed line in Fig. 13 was the secondary – tertiary stage transformation point. The standup time was estimated 10 min from the creep curve.

The models at slope inclination at 18° and 15° less than the interface's friction angle were totally undercut and still in stable. The undercut width and the slope inclination caused the difference of standup time. Figs. 14 graphically summarize the standup time of long term creep of the numerical simulations. Table 3 tabulates the standup time of the series at a various undercut width.

Comparing the standup time, the standup times were obviously shorter when the undercut width was extended. At the same undercut width, the standup times of the steeper slopes were, obviously, less than the shallower.

It is noted that the standup time were numerically estimated at undercut width not wider than 0.3 m for slope inclination 50° and 0.4 m slope inclination 30° models. The cause would probably be an infinitesimal standup when the undercut width approached the maximum.

Stress changes in the undercut slope models were also investigated during the creep stage transition, from secondary to tertiary creep stage. Fig. 15 presents the radial and tangential stresses at Zs and Hs points of an inclination 50° undercut slope model (#1 model), as an example. The radial and tangential stresses were nearly constant in the secondary creep stage. The creep stage initially changed from secondary to tertiary creep stage when the creep time was approaching 10 min, its standup time. During the transition, the stresses started to decrease, and the creep rate began to increase non-linearly. At the beginning of the tertiary creep stage, the stresses returned to increase with high creep rate. Finally, the slope model was totally failed.

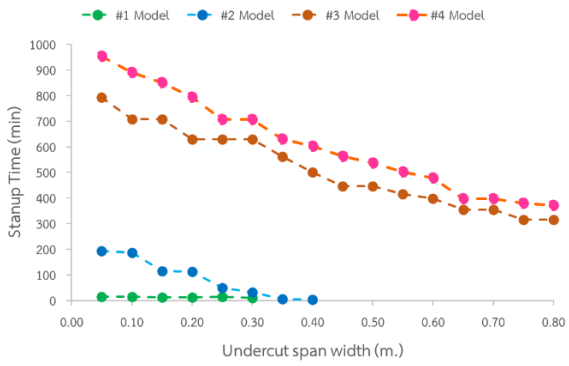

Fig.14 Standup time of long term creep behavior.

Table 3. Standup time of the models at the maximum undercut width.

Creep model	Model ID	Slope inclination (°)	Undercut width (m)	Standup time (min)
Long term creep	#1	50	0.30	10
	#2	30	0.40	2.8
	#3	18	0.80	316
	#4	15	0.80	371

Stress changes in the undercut slope models were also investigated during the creep stage transition, from secondary to tertiary creep stage. Fig. 15 presents the radial and tangential stresses at Zs and Hs points of an inclination 50° undercut slope model (#1 model), as an example. The radial and tangential stresses were nearly constant in the secondary creep stage. The creep stage initially changed from secondary to tertiary creep stage when the creep time was approaching 10 min, its standup time. During the transition, the stresses started to decrease, and the creep rate began to increase non-linearly. At the beginning of the tertiary creep stage, the stresses returned to increase with high creep rate. Finally, the slope model was totally failed.

5. Conclusions.

In this paper, creep deformation of undercut slopes was studied by using a set of numerical models. The assigned physical properties including creep properties for the numerical models were determined in laboratory tests. Mohr-Coulomb and Burgers visco-plastic models revealed the changes of stresses and deformations of undercut slopes. The models were constructed in four different dip angles of inclined rigid bed or slope, which were 50°, 30°, 18° and 15°.

Based on the Mohr-Coulomb model results, the change of stresses in undercut slopes confirmed the previous studies. When the slope was undercut, the major and minor principal stresses were altered in magnitude and directions. The directions of the major and minor principal stresses were switched and became the tangential and radial stresses, respectively. The major principal stress, in the circumferential of the arch, supported the slope. While the minor principal stress, in radial direction, confined the arch and aligned.

The maximum undercut width depended on the slope inclination and interface friction angle between the moist sand and the inclined bed. The wider undercut width had more extent when the slope inclination was shallowed. When the

inclination angle, for example 18° and 15°, was less than the interface friction angle (18.5°) between the moist sand and the inclined bed, the slope toe was totally undercut, and the slope was still in stable.

For creep analyses, all models, assigned Burgers creep model, slowly displaced, and ultimately failed. The Fig.16 shows displacement magnitude of creep models at maximum undercut width. The undercut width and the slope inclination affected the stresses in undercut slopes that greatly affected the standup time. The standup time of an undercut slope was shorter when the undercut width was extended. At the same undercut width, the standup times of the steeper slopes were, clearly, less than the shallower.

In the future study, the stress changes in the undercut during tertiary creep stage transition need further investigations. Physical models could be the first priority. The creep of undercut slope models would give an interesting information that would help us to have more understanding of creep deformation of undercut slopes

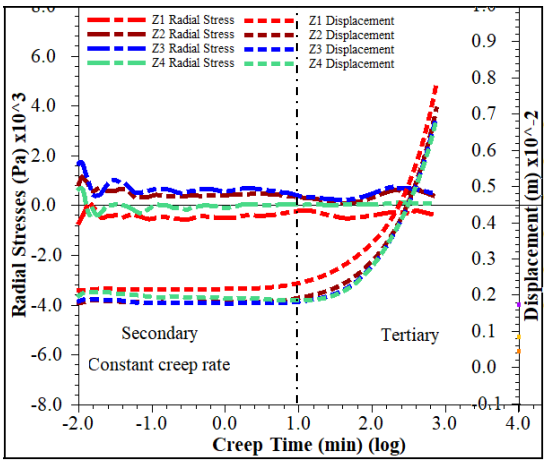

a) Radial stress and displacement rate of Zs points.

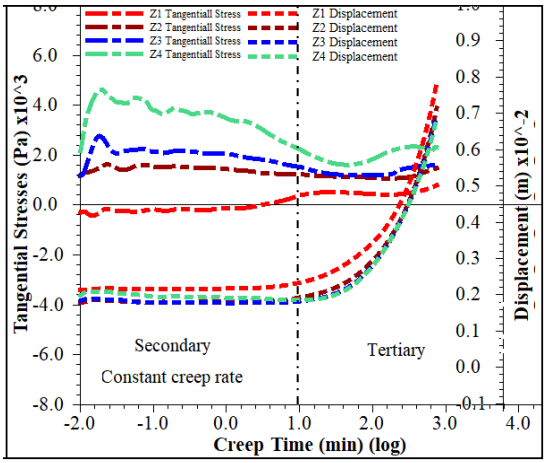

b) Tangential stress and displacement rate of Zs points.

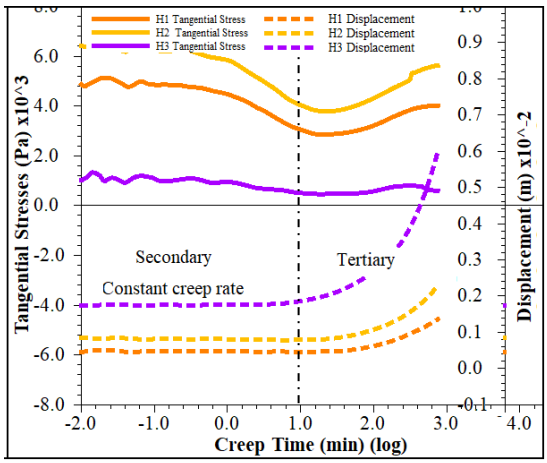

c) Tangential stress and displacement rate of pillars at H1, H2 and H3 points

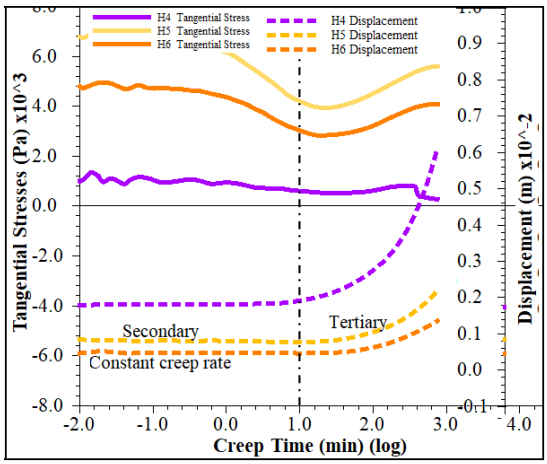

d) Tangential stress and displacement rate of pillars at H4, H5 and H6 points

Fig. 15 Stresses, displacements and creep time of #1 model with undercut width 0.30 m.

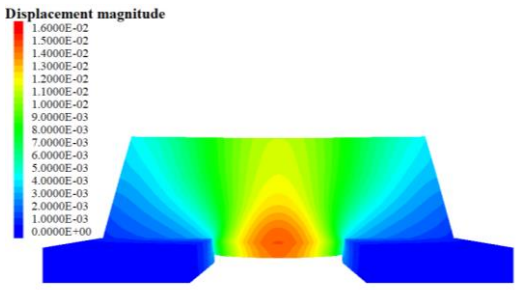

a) 0.30 m undercut width at 50° slope inclination.

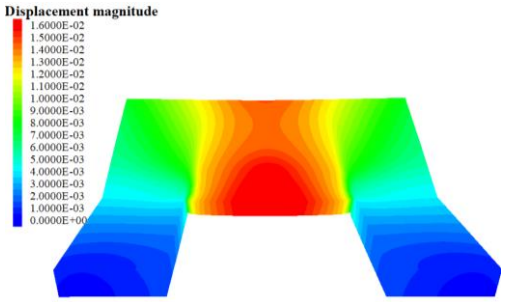

b) 0.40 m undercut width at 30^{o} slope inclination.

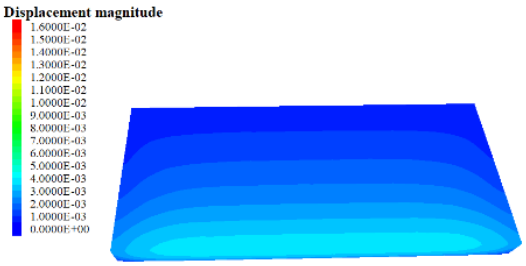

c) 0.80 m undercut width at 18^{o} slope inclination

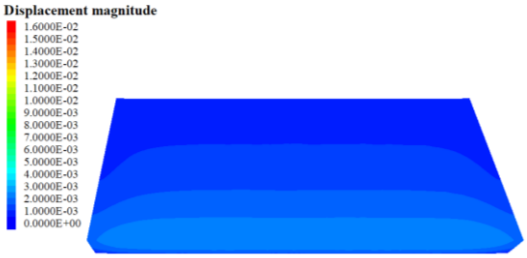

d) 0.80 m undercut width at 15^{o} slope inclination.

Fig.16 Displacement magnitude of Burgers creep models.

References

[1] Pipatpongsa, T., Khosravi, M., Takamura, J. & Leelasukseree, C., 2016. Modelling concepts of passive arch action in undercut slopes. In Proceedings of APSSIM 2016 in Australian Center for Geomechanics, 507-520. Brisbane: Australia.

[2] Khosravi, M. et al., 2012. Performance of counterweight balance on stability of undercut slope evaluated by physical modeling. J.Geotechnical Engineering Res 6:2 193-205.

[3] Itasca Consulting Group, 2016. 3DEC 3dimensional distinct element code user's guide. USA: Itasca Consulting Group, Inc.

[4] Dowling, N. E., 2012. Mechanical Behavior of Materials. England: Pearson Education Limited.

[5] Brady, B. H. G. & Brown, E. T., 2004. Rock Mechanics for underground mining. United States of America: Springer Science + Business Media, Inc.

[6] Altenbach, H. & Naumenko, K., 2006. Modeling of creep for structural analysis. s.l.:Springer Berlin Heidelberg New York.

[7] Goodman, R. E., 1989. Rock mechanics second Edition. Canada, 202-210.

[8] Wgllie, D. C. & Mah, C. W., 2005. Rock slope engineering civill and mining 4 th edition. New York: Taylor & Franics e-Library.

[9] Das, B.M, 1984. Fundamentals of Geotechnical Engineering. United States: Chris carson.

[10] Ukritchon, Ouch, R., B. & Pipatpongsa, T., 2017. Investigation of Stability and Failure Mechanism of Undercut Slopes by Three-Dimensional Finite Element Analysis. KSCE journal of Civil Engineering, 4 August